Kinetics of the Light-Induced Proton Translocation Associated with the pH-Dependent Formation of the Metarhodopsin I/II Equilibrium of Bovine Rhodopsin†

Stefan Dickopf, Thorsten Mielke, and Maarten P. Heyn*

Biophysics Group, Department of Physics, Freie Universität Berlin, Arnimallee 14, D-14195 Berlin, Germany

Received August 5, 1998; Revised Manuscript Received September 21, 1998

ABSTRACT: The kinetics of the formation of the meta$_{II}$ (M_{II}) state of bovine rhodopsin was investigated by time-resolved electrical and absorption measurements with rod outer segment (ROS) fragments. Photoexcitation leads to proton transfer in the direction from the cytosolic to the intradiscal side of the membrane, probably from the Schiff base to the acceptor glutamate 113. Two components of comparable amplitude are required to describe the charge movement with exponential times of 1.1 (45%) and 3.0 ms (55%) (pH 7.8, 22 °C, 150 mM KCl). The corresponding activation energies are 86 and 123 kJ/mol, respectively (150 mM KCl). The time constants and amplitudes depend strongly on pH. Between pH 7.1 and 3.8 the kinetics becomes much faster, with the faster and slower components accelerating by factors of about 8 and 2, respectively. Complementary single-flash absorption experiments at 380 nm and 10 °C show that the formation of M_{II} also occurs with two components with similar time constants and pH dependence. This suggests that both signals monitor the same molecular events. The pH dependence of the two apparent time constants and amplitudes of the optical data can be described well over the pH range 4−7.5 by two coupled equilibria between M_I and two isochromic M_{II} species M_{IIa} and M_{IIb}: $M_I \underset{k1}{\overset{k0}{\rightleftharpoons}} M_{IIa}(380) \underset{k3}{\overset{k2}{\rightleftharpoons}} M_{IIb}(380)$, with k_0 proportional to the proton concentration. This model implies that deprotonation of the Schiff base and proton uptake are tightly coupled in ROS membranes. Models with k_2 proportional to the proton concentration cannot describe the data. Photoreversal of M_{II} by blue flashes (420 nm) leads to proton transfer in a direction opposite to that of the signal associated with M_{II} formation. In this transition the Schiff base is reprotonated, most likely from glutamate 113. At pH 7.3, 150 mM KCl, 22 °C, this electrical charge reversal has an exponential time constant of about 30 ms and is about 10 times slower than the forward charge motion.

Rhodopsin, the photoreceptor of rod cells, is a member of the large family of G-protein coupled receptors with the structural motif of a transmembrane heptahelical bundle (for reviews see refs *1*−*3*). In the dark the retinylidene chromophore is covalently linked to lysine 296 of opsin via a protonated Schiff base and is in the 11-cis configuration. Absorption of light leads to rapid photoisomerization of the chromophore to the all-trans form. This is followed by a series of slower structural relaxations that lead after several milliseconds to receptor activation in the transition from metarhodopsin I (M_I)[1] to M_{II}. This step is accompanied by deprotonation of the Schiff base, proton transfer to glutamate 113 (*4*), and the uptake of protons in the cytoplasmic loop domain (*5*−*9*). We have studied the kinetics of the proton transfer using time-resolved absorption and electrical measurements. The formation of the deprotonated Schiff base in M_{II} leads to a large blue shift in the chromophore absorption maximum (380 nm), which may be used to monitor the kinetics of this local charge transfer. The kinetics of charge movements near the chromophore and elsewhere may be monitored using transient photovoltage measurements. In such experiments the signal amplitude is proportional to the charge displacement distance divided by the local dielectric constant (*10*). In principle both the intramolecular H^+ transfer from the Schiff base to the acceptor glutamate 113 and the proton uptake at the cytoplasmic surface may contribute to the electrical signals on the millisecond time scale. Molecular recognition and binding of transducin occur to the altered structure of the cytoplasmic loop domain in the M_{II} state. An important unresolved question is how the initial events in the chromophore region, which is deeply buried in the middle of the protein, are transmitted to the surface loop domain. Of particular interest is thus the question of a possible coupling between the deprotonation of the Schiff base and the proton uptake at the membrane surface. We have therefore studied the pH dependence of the charge motion using bovine ROS membranes in the pH range from 4 to 9. Although electrical measurements on the millisecond time scale have been performed previously (*11*−*15*), the pH dependence of these signals has surprisingly received little attention. The pH dependence of the optical signals has been

† This work was supported by Grant Sfb 312-B1 from the Deutsche Forschungsgemeinschaft (to M.P.H.).

* Address correspondence to this author. Phone +49-30-838 6174; Fax +49-30-838 6299; Email heyn@physik.fu-berlin.de.

[1] Abbreviations: ROS, rod outer segment; DTT, dithiothreitol; M_I, metarhodopsin I; M_{II}, metarhodopsin II; Tris, tris(hydroxymethyl)-aminomethane; HEPES, *N*-(2-hydroxyethyl)piperazine-*N*′-2-ethanesulfonic acid; SDS, sodium dodecyl sulfate.

10.1021/bi981879m CCC: $15.00
Published on Web 11/12/1998

investigated in the past, but only over a narrow pH range and with low time resolution (*8*). We observed two apparent rate constants in the kinetics of both the electrical and optical signals. The faster of these accelerated strongly with decreasing pH. The amplitudes and rate constants were modeled over the whole pH range with one set of four microscopic rate constants. The model is based on two sequential equilibria between M_I and two isochromic species M_{IIa} and M_{IIb} with the pH dependence residing in the first forward rate constant between M_I and M_{IIa}. This result suggests a strong coupling between the formation of M_{IIa} and proton uptake at the surface. When M_{II} was excited with blue flashes (420 nm), a photovoltage of opposite sign was observed, suggesting that the Schiff base is reprotonated from glutamate 113. With a time constant of 30 ms this reversed proton transfer is surprisingly slow.

MATERIALS AND METHODS

Sample Preparation. The eyes of freshly slaughtered cows were collected in a cooled light-tight container. After preparation of the retinas, the ROS membranes were isolated at low ionic strength as described (*16*) and purified over a stepwise sucrose density gradient. To remove the other peripheral proteins of the visual cascade (e.g., transducin, arrestin, rhodopsin kinase, and phosphodiesterase) the ROS membranes were washed with 4 M urea as described (*17*). The washed membranes were resuspended in 3 mM Tris, 3 mM HEPES, 3 mM sodium acetate, pH 7.5, 150 mM KCl, and 1 mM DTT and stored at −80 °C under argon. SDS−polyacrylamide electrophoresis showed that, after the washing procedure, the band due to the α-subunit of transducin was absent.

Flash Photolysis. Washed ROS membranes were suspended in 3 mM Tris, 3 mM HEPES, 3 mM sodium acetate, pH 7.5, and 150 mM KCl at a final concentration of 0.3 mg of rhodopsin/mL and the pH was set in the range 4.0−9.0 by the addition of KOH or HCl. Measurements of the time-resolved absorption changes after flash excitation were performed as described (*18*). Absorption spectra were recorded before and after each single-flash transient absorption experiment.

Time-Resolved Photovoltage Measurements. The time-resolved measurements of the electrical charge displacement were performed with the method of capacitative coupling, in which ROS fragments are adsorbed to a lipid-impregnated support foil, as described (*19*−*21*). In the cuvette for the electrical measurements the two compartments are separated by a 2 μm thick polyethylene foil (Hostaphan RE2, Hoechst Diafoil, Wiesbaden, Germany). This foil is impregnated on one side with a solution of 1% (w/v) L-1,2-diphytanoyl-3-phosphatidylcholine (Avanti Polar Lipids, Birmingham, AL) and 0.025% octadecylamine (Fluka, Buchs, Switzerland) in *n*-decane (Merck, for gas chromatography). After evaporation of the solvent, the foil is coated by a lipid layer that carries a positive surface charge. The compartments are filled with a solution containing 3 mM Tris, 3 mM HEPES, 3 mM sodium acetate buffer, and 150 mM KCl. A concentrated ROS membrane suspension (about 5 mg of rhodopsin/mL) is briefly sonicated (20 s) to produce ROS membrane fragments. A 40 μL aliquot of the sonicated suspension is added to the compartment on the coated side of the foil. The amount of rhodopsin in the cuvette is then about 5 nmol. The electrical signal that is generated in this experimental setup after photoexcitation by a 10 ns pulse (532 nm) from a frequency-doubled Nd−YAG laser (GCR 16, Spectra Physics) is measured with Pt electrodes. For the photoreversal experiments an excimer laser-pumped dye laser was used at 420 nm (10 ns). The data acquisition system with logarithmic time base was as described (*20*).

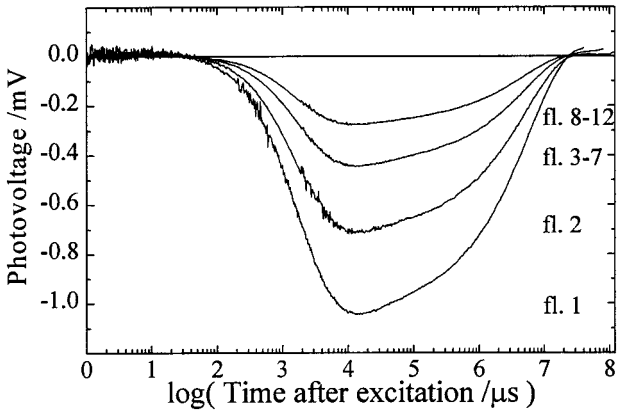

FIGURE 1: Time-resolved photovoltage signal of ROS membrane fragments after excitation by 532 nm flashes (5 mJ, 10 ns). Note the logarithmic time scale. Time traces are shown after the first and second flashes. The signals due to flashes 3−7 and 8−12 were averaged. Differences in signal-to-noise ratio are due to different sampling rates. Conditions: pH 7.8, 150 mM KCl, 22 °C.

RESULTS

Time-Resolved Charge Displacement. Figure 1 shows the time-resolved photovoltage of adsorbed ROS membrane fragments after excitation by 532 nm flashes (5 mJ) at pH 7.8, 150 mM KCl, 22 °C. The trace following the first flash provides evidence that electrical data of excellent signal-to-noise ratio can be obtained from a single flash. Due to the formation of M_{II} by the first flash, the signal amplitude following the second flash is 30% smaller than after the first flash. Figure 1 shows that with increasing number of flashes the signal is progressively reduced by this bleaching effect. The main phase of charge translocation occurs in the time range from 100 μs to 10 ms and was fitted with two exponentials with time constants of 1.1 and 3.0 ms and amplitudes of 45% and 55%, respectively. Alternatively the kinetics can be described by a Gaussian distribution of exponentials (*19*) with a mean time of 1.9 ms and a width σ of 0.24. At this pH the quality of the fits with the two model functions is about equal. With decreasing pH the separation between the two time constants increases and at low pH a fit with two exponentials is clearly superior over a fit with distributed kinetics (see below). The time constants of the kinetics are unaltered in the series of subsequent flashes of Figure 1. This observation indicates that electrical signals due to the excitation of long-living intermediates are absent. After 10 ms the transient photovoltage decays again in several phases. This system discharge is well understood (*19*) and is due to the external resistance and the membrane conductivity. The system discharge starts already with a 60 ms component, considerably earlier than in the case of purple membranes (longer than 1 s under comparable conditions). This is probably due to a weaker adsorption of the ROS fragments to the support.

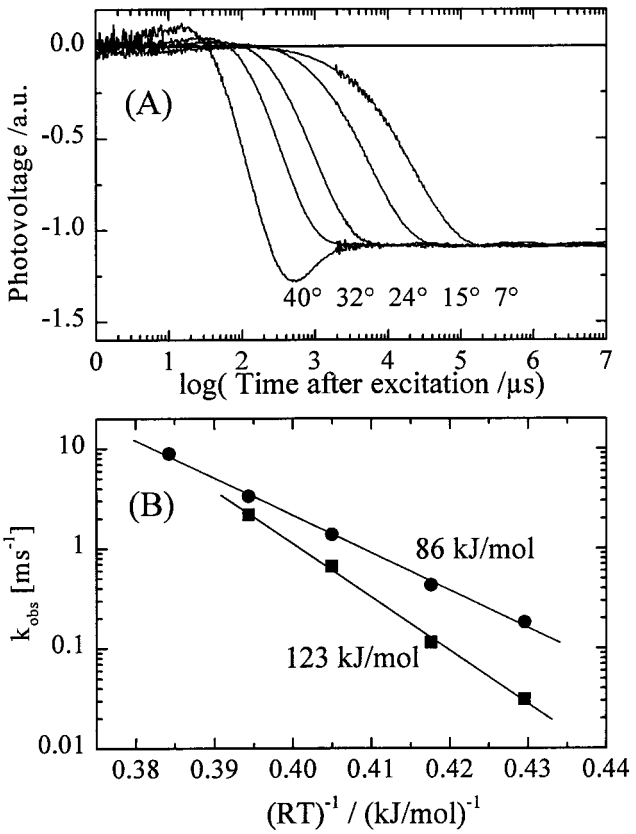

FIGURE 2: (A) Temperature dependence of the kinetics of the photovoltage. The temperature was varied from 7 to 40 °C. With increasing temperature the system discharge time decreases from 1 s at 7 °C to 10 ms at 40 °C. The system discharge was subtracted as described (*19*). The overshoot at 40 °C is probably an artifact due to the very early onset of the system discharge. Conditions: pH 7.8, 150 mM KCl. (B) Arrhenius plot of the fast (●) and slow (■) apparent rate constants of the photovoltage. The slower component has the larger activation energy of 123 kJ/mol.

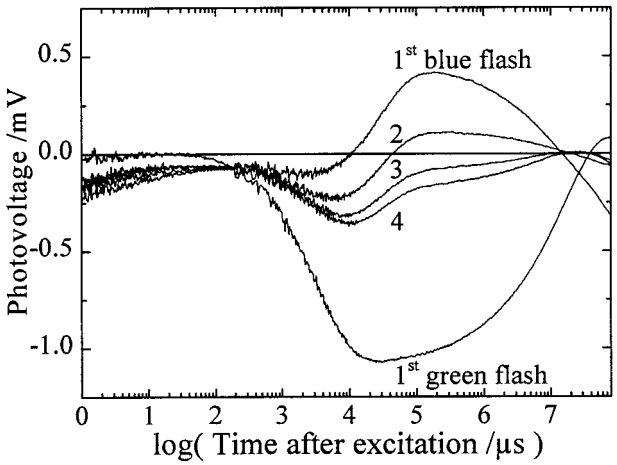

FIGURE 3: Kinetics of the charge movement (photovoltage) associated with the photoreversal of M_{II} by a blue flash (420 nm). The sample was first excited by a strong green flash (532 nm) leading to incomplete (partial) formation of M_{II} and generation of the corresponding photovoltage (largest negative trace). The sample was then completely converted within 1 minute to the M_I/M_{II} equilibrium by a series of 19 further green flashes. The sample was immediately afterward excited by a series of four blue flashes (420 nm, 2 mJ, 10 ns), which led to reisomerization of the chromophore and reprotonation of the Schiff base. Conditions: pH 7.3, 150 mM KCl, 22 °C.

The negative sign of the transient photovoltage means that positive charge moves toward the support membrane. The osmotic stress induced by the prolonged washing in 4 M urea together with the sonication procedure will lead to ROS membrane fragments. These will adsorb with their intradiscal side to the positively charged support since it was recently shown that the extradiscal membrane is positively charged (*29*). For the same reason intact discs, should they still be present in the preparation, would not adsorb. The only known charge motions associated with the rise of M_{II} (millisecond time range) are proton transfer from the Schiff base to Glu 113 and proton uptake at the cytosolic surface. Although no structure of rhodopsin is available at atomic resolution, all molecular modeling studies that take into account a number of constraints from biophysical measurements conclude that the carboxyl group of Glu 113 is located between the Schiff base and the intradiscal membrane (*22*−*24*). Both of the above reactions thus involve proton displacement in the direction from the cytosolic to the intradiscal surface. The observed sign of the photovoltage is therefore consistent with the preferred adsorption of the ROS membrane fragments with their intradiscal side to the positively charged support.

As shown in Figure 2A, the kinetics of the photovoltage is strongly temperature-dependent. In this figure the system discharge has been subtracted according to standard procedures (*19*). The overshoot component of opposite sign at 40 °C is probably an artifact due to the early onset of the system discharge at this temperature. The time traces were fitted either with two exponentials or with a Gaussian distribution of exponentials. From the Arrhenius plots, activation energies of 123 and 86 kJ/mol were obtained for the slow (■) and fast (●) exponential components, respectively (Figure 2B). The Gaussian distribution led to an activation energy of 121 kJ/mol.

Absorption of blue light in the M_{II} state leads to photoreversal to the initial unphotolyzed state of rhodopsin and is accompanied by reisomerization of the chromophore, reprotonation of the Schiff base, and proton release (*25*, *26*). To measure the proton charge displacement associated with this reaction, the adsorbed ROS fragments were first completely bleached within 1 min by a rapid succession of 20 intense green flashes at 532 nm. The lowest trace of Figure 3 shows the normal 2 ms proton motion associated with the formation of M_{II} induced by the first green flash of this sequence. After 20 green flashes no photovoltage could be detected anymore, suggesting that all of the rhodopsin had been converted to the M_I/M_{II} equilibrium. Under the conditions of this experiment (pH 7.3 and 22 °C), the lifetime of M_{II} is about 10 min. Immediately after the bleaching by the green flashes, a blue flash (420 nm) induced the photo backreaction from M_{II}. The trace labeled first blue flash in Figure 3 shows that, following this flash, the photovoltage is of positive sign, suggesting that protons move in a direction opposite to that induced by the first green flash. A rise time of 30 ms was obtained by fitting with a single exponential. The decay starting after 200 ms is due to the system discharge. Additional blue flashes lead to a reduction of the positive reversal signal (Figure 3, traces 2−4). This is due to the decrease in the amount of available photoreversible M_{II}, as a consequence of the photoreversal to the initial state. These traces show, moreover, that after the first blue flash a

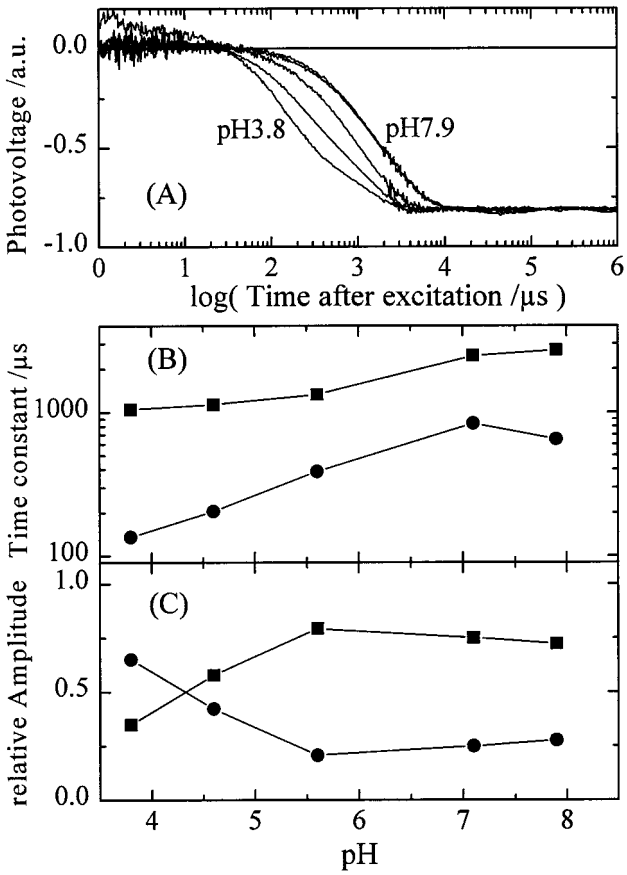

FIGURE 4: (A) pH dependence of the kinetics of the photovoltage of ROS membranes after excitation by green flashes (532 nm). The system discharge was subtracted. The titration was performed from high to low pH with aliquots of H_2SO_4. The pH decreases from 7.9 for the trace on the right to 3.8 for the trace on the left with intermediate values of 7.1, 5.6, and 4.6. The traces at pH 7.9 and 7.1 are virtually identical. The signals were scaled to the same amplitude. (B) Dependence of the two apparent fast (●) and slow (■) time constants on pH. The data of panel A were fitted with two exponentials at each pH. (C) Dependence of the relative amplitudes of the fast (●) and slow (■) component on pH. Conditions: 150 mM KCl, 22 °C.

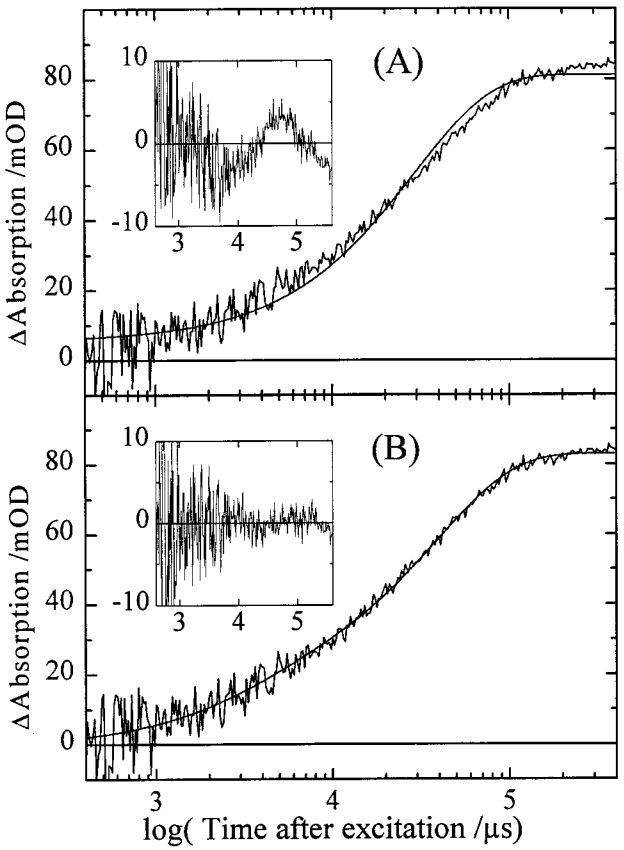

FIGURE 5: Kinetics of the absorbance change at 380 nm associated with the formation of M_{II} in ROS membranes at pH 5.5, 150 mM KCl, 10 °C. Excitation was by a single 532 nm flash (5 mJ, 10 ns). (A) Fit of the data with one exponential. Inset: residuals. (B) Fit of the data with two exponentials. Inset: residuals.

negative photovoltage starts to build up with the same shape and 2 ms time constant as the signal induced by the first 532 nm green flash. This is due to the photoexcitation by the blue flashes of the rhodopsin regenerated by the photoreversal of M_{II}. The traces after the second, third and fourth blue flashes are thus superpositions of contributions from the photoreversal of M_{II} (positive) and from the build-up of M_{II} (negative).

The kinetics of the millisecond charge displacement is markedly pH-dependent. The data of Figure 4A show that with decreasing pH (22 °C, 150 mM KCl) the kinetics accelerates by about an order of magnitude. Curve-fitting with two exponentials at each pH leads to the pH dependence of the two time constants presented in Figure 4B. The faster time constant is pH-independent above pH 7 and becomes increasingly faster with decreasing pH. The slower time constant is only weakly pH-dependent. Thus at pH 3.8 the two time constants differ by about a factor of 10. An analysis of the residuals shows that at this pH curve-fitting with distributed kinetics is clearly inferior compared to fitting with two exponentials. The break in the slope of the time trace at pH 3.8 (Figure 4A, logarithmic time scale) also provides strong evidence for the existence of two components. The same adsorbed sample was used throughout this pH series. The sample was therefore progressively bleached. In contrast to absorption measurements, the amount of remaining unphotolyzed material cannot be determined in electrical measurements. The amount of adsorbed material may also be pH-dependent. For these reasons no reliable absolute amplitudes can be obtained from the electrical data. The data of Figure 4A are therefore scaled to the same end value. It is, however, possible to determine the relative amplitudes of the two components and these data are plotted in Figure 4C. From this panel it is apparent that below pH 4.5 the faster component has the largest amplitude. Above this pH the opposite is the case.

Flash Spectroscopy. Since the observed charge movement is most likely due to proton transfer from the Schiff base to Glu 113 in the formation of M_{II}, it is of great interest to compare the photovoltage kinetics with the kinetics of the absorbance change at 380 nm, which monitors the rise of M_{II}. These measurements were performed at 10 °C to slow the kinetics sufficiently to get single-flash traces of adequate signal-to-noise ratio. Due to the very strong light scattering by ROS membrane fragments, the signal-to-noise ratio in single-flash experiments is much worse in the optical than in the electrical measurements. Figure 5 shows a single-flash trace for the absorbance increase at 380 nm due to the formation of M_{II} at pH 5.5 in the time window from 400 μs to 400 ms. Panel A shows that a fit with a single exponential leads to systematic deviations as evidenced by the residuals

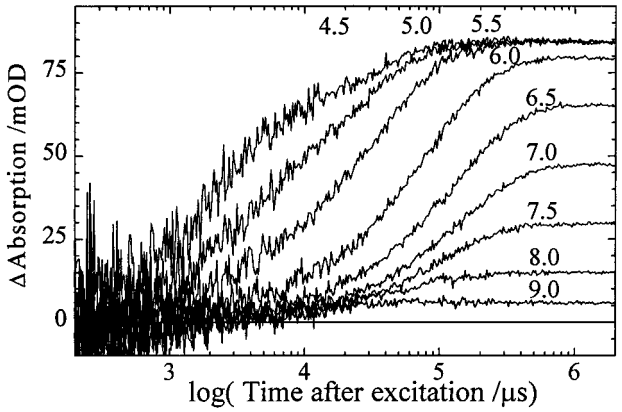

FIGURE 6: pH dependence of the kinetics of the absorbance changes at 380 nm after excitation of ROS membranes by a single 532 nm flash. At each pH a fresh aliquot of the same sample was used. For clarity of presentation the signal at pH 4.0 is not shown. The signals at pH 5 and 4.5 were scaled by factors of 1.08 and 1.25, respectively, to the same final amplitude at 1 s after the flash. Conditions: 150 mM KCl, 10 °C.

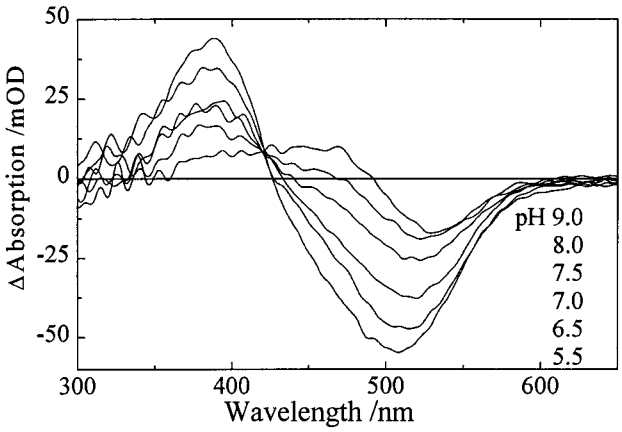

FIGURE 7: Difference spectra of ROS membranes before and after each single-flash kinetic experiment of Figure 6. At each pH a fresh sample of the same rhodopsin concentration was used. With decreasing pH the amplitude of the absorbance changes at 510 and 400 nm increases due to the pH dependence of the M_I/M_{II} equilibrium. Conditions: 150 mM KCl, 10 °C.

(inset). A satisfactory fit (panel B) at this signal-to-noise ratio requires two exponentials. These experiments were repeated for 10 pH values from pH 9 to 4. The data are presented in Figure 6. It is apparent from this figure that after around 1 s the M_I/M_{II} equilibrium is fully established. The clear break in the slope of the trace at pH 4.5 is further evidence for the existence of two kinetic components with comparable amplitudes. Care was taken to reduce the intensity of the measuring beam at 380 nm sufficiently to avoid photo-back-reactions from M_{II}. This would lead to a reduction in the absorption signal at 380 nm. Under our experimental conditions such effects were observable after about 6 s. The measuring beam was turned on less than 2 s before the 532 nm flash. To prevent complications from photoreactions from long-living intermediates, a fresh aliquot from the same preparation was used at each pH and only the data from the first flash were used. Spectra were taken before and after each single-flash transient absorption measurement. Six of these difference spectra are shown in Figure 7 (pH 9−5.5). The amplitudes of these spectra are smaller than the corresponding constant levels reached in Figure 6, since the data acquisition was continued for 20 s. During this time the absorbance at 380 nm is reduced due to the photo-back-reaction induced by the measuring light. The amplitudes of the spectra in Figure 7 are thus reduced with respect to those in Figure 6 by a constant scaling factor. The spectra of Figure 7 indicate that at pH 9.0 the yield of M_{II}/M_I is low and that the equilibrium is on the M_I side. With decreasing pH the amplitudes at 500 and 380 nm increase and the equilibrium shifts to M_{II}. Accordingly the end value of the amplitude of the time-resolved data at 380 nm increases from pH 9 to 5.5 (Figure 6). Below pH 5.5 the amplitude decreases somewhat. Since the equilibrium is completely on the M_{II} side, this decrease may just be due to a small degree of acid denaturation. In this connection we note that the pH was adjusted just before the start of the single-flash measurements, to reduce the time of exposure to the low pH. Test experiments showed that the kinetic results were the same whether sonicated or unsonicated samples were used. Since the electrical experiments were performed with sonicated samples, this is an important point when the kinetic results obtained from the two methods are compared.

The most striking aspect of the data of Figure 6 is that the formation of M_{II} accelerates strongly with decreasing pH. The two-exponential fit described above was performed at each pH. The dependence of the two apparent time constants and the corresponding amplitudes on pH is shown in Figure 8, panels A and B, respectively. At the extremes of pH only one exponential suffices to describe the data, but in the interval from pH 4 to 7.0 two components are required. The faster component accelerates strongly from pH 6.5 to 4, whereas the slower component has a much weaker pH dependency. The pH dependence of these two optical time constants thus parallels closely that of the electrical time constants (Figure 4B). The relative amplitudes of the fast and slow components are plotted in Figure 8C as a function of pH. Upon comparison of this panel with the pH dependence of the relative amplitudes of the fast and slow electrical signals (Figure 4C), a striking similarity becomes evident. It is therefore very likely that both signals are due to the same reactions. For the data points of the fast time constant at pH 6, 6.5, and 7.0, only the upper half of the error bars are shown in Figure 8A. For these pH values the corresponding amplitudes are small and the errors in the time constants thus are large. Due to the logarithmic vertical scale the lower half of these error bars cannot be represented correctly. At pH 7.5 the amplitude of the fast component is negligible and the data were fitted with only one (slow) component. At pH 8.0 and 9.0 the total amplitude of the absorbance change is so small (see Figure 6) that a fit of the data was pointless. There are therefore no points corresponding to these pH values in Figure 8. From visual inspection of the time traces at pH 8 and 9 of Figure 6, it appears that the formation of M_{II} is faster at these pH values than at pH 7.5. In this pH range the fast so-called M_I380 intermediate may start to play an important role (*41*).

Kinetic Model. The pH dependence of the apparent time constants and amplitudes was analyzed by using kinetic models based on current ideas about the M_I/M_{II} equilibrium (*9*, *27*, *28*). In most of these models two spectrally indistinguishable intermediates with absorption maxima at 380 nm are postulated. Various nomenclatures are in use. Since we do not want to introduce new nomenclature, we will call

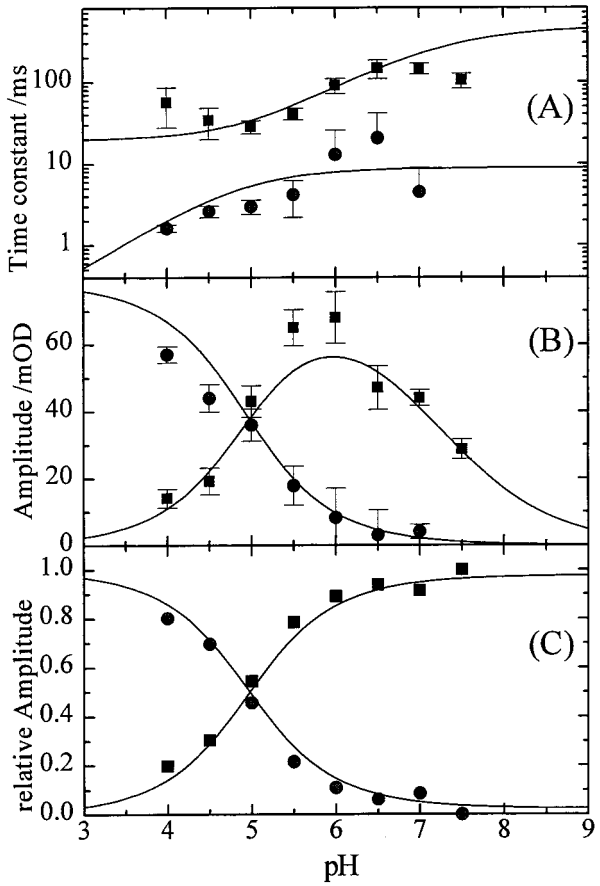

FIGURE 8: Global fit of the observed time constants (A) and corresponding amplitudes (B) for the 380 nm absorbance change of M_{II} from pH 4 to 7.5. (●, ■) Experimental values for the fast and slow components; (—) global fit according to the kinetic model of eq 1 and the Appendix. The values of the microscopic rate contants k_0, k_1, k_2, and k_3 of the global fit are given in the text and in the inset of Figure 9. The relative amplitudes of the fast (●) and slow (■) components are plotted in panel C together with the global fit (—).

these isochromic species M_{IIa} and M_{IIb} according to ref *9*. We observed only two time constants in both our electrical and optical data. Therefore the following kinetic model is sufficient to describe our data:

$$M_I \underset{k_1}{\overset{k_0}{\rightleftharpoons}} M_{IIa}(380) \underset{k_3}{\overset{k_2}{\rightleftharpoons}} M_{IIB}(380) \qquad (1)$$

Analytical solutions for the two apparent time constants and amplitudes in terms of the four microscopic rate constants were derived for the kinetic scheme of eq 1 and the results are summarized in the Appendix. The pH dependence of the rate constants could reside either in k_2 or in k_0. We found that models with k_2 proportional to some power of $[H^+]$ could not describe the observed pH dependence. In such models the rate k_2 increases with decreasing pH and ultimately becomes faster than k_0. Below a critical pH k_0 will thus become rate-limiting in the rise of the absorbance signal at 380 nm (due to the formation of M_{IIa} and M_{IIb}). The rise of the signal will not become faster when the pH is lowered below this critical value. No such limitation was observed in the pH range explored (see Figure 8). Moreover, this model implies that at low pH the whole amplitude of the M_{II} build-up will occur with the slower k_0 rate. This is contrary to the data (Figure 8), which show that at low pH

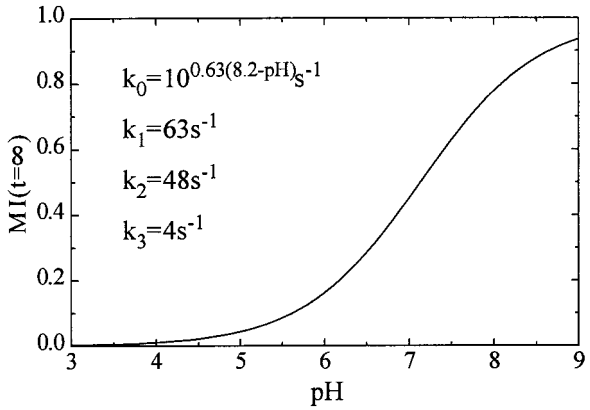

FIGURE 9: pH dependence of the equilibrium amount of M_I calculated according to eq 14 of the appendix with the best-fit values for $\{k_0, k_1, k_2, k_3\}$ from the global fit (inset). Conditions: 10 °C, 150 mM KCl. The apparent p*K* is 7.14 (calculated from eq 15 of the Appendix).

the amplitude of the faster component dominates. Furthermore, with this model, the amplitude of the faster component reaches a constant value at high pH, also contrary to our observations.

Models with k_0 proportional to some power of $[H^+]$ are successful, however, in describing the dependence of the time constants and amplitudes over the whole pH range. The amplitudes and apparent time constants were fitted at all pH values simultaneously with one set of six parameters: the four rate constants, the exponent n in $k_0 \sim [H^+]^n$, and an optical parameter (see Appendix). The results of the global fit are shown in Figure 8 (lines). The agreement between data and fit is quite satisfactory, also in view of the errors in the kinetic parameters. For the time constants the error bars are of course quite large when the corresponding amplitudes become small. We noted that the data in Figure 6 at pH 4.0, 4.5, and 5.0 were scaled to bring them to the same end value for long times. In the points of Figure 8B these scaling factors were not taken into account. Using these scaling factors as correction factors would improve the agreement between the amplitudes and the model (—) considerably for these pH values. This is evident from Figure 8C, where the fit to the relative amplitudes is much improved compared to Figure 8B (absolute amplitudes) for the low pH points. The relative amplitudes are of course independent of the overall scaling factor.

At 10 °C and 150 mM KCl, the best rate constants from the global fit are $k_0 = 10^{0.63(8.2-pH)}$ s^{-1}, $k_1 = 63$ s^{-1}, $k_2 = 48$ s^{-1}, and $k_3 = 4$ s^{-1}. With these values the equilibrium between M_{IIa} and M_{IIb} is on the side of M_{IIb} and pH-independent, while the equilibrium between M_I and M_{IIa} is pH-dependent. The noninteger value of $n = 0.63$ is probably due to the surface charge, which leads to a pH-dependent difference between the bulk and surface pH (see Discussion). Using the microscopic rate constants from the global fit, the equilibrium concentration of M_I can be calculated at every pH according to eq 14 of the appendix. The resulting titration curve, shown in Figure 9, has the form of the Henderson—Hasselbalch equation with an apparent p*K* given by eq 15 of the Appendix. Substituting the values obtained for the microscopic rate constants, we calculate an apparent p*K* of 7.14, in excellent agreement with the value of 7.3 obtained for ROS membranes under the same conditions (*29*).

DISCUSSION

Nature and Kinetics of the Charge Displacement. The kinetics of the electrical signal associated with the rise time of M_{II} has been investigated by using collodion films (*12*), cellulose filters (*11*, *13*, *15*) or black lipid membranes (*14*) as the adsorbing and orienting support. The authors of ref *13* found that the kinetics could be best described by a distribution of rates and fitted their data with a power law. At 30 °C (pH 7, 100 mM NaCl) they obtained a peak time constant of 2.2 ms ($n = 1.5$). Under similar conditions (22 °C, pH 7.8, 150 mM KCl) two components with time constants of 1.1 and 3.0 ms and comparable amplitudes were required to fit our data. In ref *12* at least two components with half-times of 500 μs and several milliseconds were needed, but these authors did not carry out a quantitative analysis of their data. In ref *14*, with poor time resolution, one time constant of 2 ms was observed (20 °C, pH 7.0). Our pH-dependent experiments show clearly that in particular at low pH two components are required rather than a distribution.

The absorbance change at 380 nm is due to the deprotonation of the Schiff base and indicates the formation of M_{II}. The proton acceptor is Glu 113 (*4*, *30*). The observed light-induced charge displacement in the millisecond time range is also due to proton transfer as suggested by the observed kinetic H/D isotope effect (data not shown). Its sign is such that it could be associated either with the proton transfer from the Schiff base to Glu 113 or with the proton uptake on the extradiscal side (Glu 134), both of which occur on this time scale. From the close similarity between the pH dependencies and activation energies of the electrical and optical signals, we conclude that the electrical signal is due to the proton transfer from the Schiff base to Glu 113. Proton uptake at the surface in an environment of higher dielectric constant is moreover expected to lead to an electrical signal of small amplitude. We therefore also interpret the reverse photovoltage in the photo-back-reaction from M_{II} as the intramolecular reprotonation of the Schiff base from Glu 113.

Temperature Dependence. We observed very large activation energies of 86 and 123 kJ/mol for the fast and slow components of the electrical signal, respectively. Such a strong temperature dependence was also reported for the absorption signal at 380 nm associated with the M_I/M_{II} transition. For ROS membranes, for example, activation energies of 67 and 107 kJ/mol were obtained for the fast and slow optical components, respectively (*28*). This similarity in temperature dependence suggests that both signals monitor the same molecular events. Activation energies of 139.5 (*13*) and 100 kJ/mol (*14*) were obtained when the electrical signal was described with a single time constant using either a power law (*13*) or a single exponential (*14*).

pH Dependence and Surface Charge Effects. An important advantage of electrical over optical measurements is that data of much better signal-to-noise ratio can be obtained with single-flash excitation. This is due to the fact that light-scattering does not contribute to the electrical signal. In this way it was established (Figure 4) that the faster component has the stronger pH dependence. A disadvantage of the electrical measurements is that no reliable absolute amplitude data can be acquired. Such data may be obtained from absorption measurements. With both methods (Figures 4A and 5) only two components were observed in single-flash experiments. Therefore the kinetic model of eq 1, which predicts two apparent time constants, is sufficient. It provides an adequate description of the pH dependence of the kinetic electrical and optical data and the equilibrium properties. More complex models will give a better fit, with more parameters. The simplest model with two equilibria and only six parameters is to be preferred, however. The strong pH dependence is due to proton uptake, most likely that occurring on the extradiscal surface (*9*, *31*). Attempts to associate this proton uptake with k_2 were unsuccessful. The pH dependence apparently resides in k_0. Since the microscopic rate constant for the transition between M_I and M_{IIa} is proportional to the external proton concentration, this means that proton uptake and deprotonation of the Schiff base are strongly coupled in ROS membranes. The formation of M_{IIa}, with deprotonation of the Schiff base and proton uptake, is in our model followed by the conversion of M_{IIa} to M_{IIb}. The later transition, associated with the larger activation energy, is probably the major structural change occurring in the activation of rhodopsin. For the related retinal protein bacteriorhodopsin, it was concluded that the loss of the electrostatic interaction between the protonated Schiff base and the counterion was the cause of the large-scale conformational change (*32*).

A similar model was used to analyze the kinetics and pH dependence of the absorbance signal at 380 nm and the proton uptake reaction for rhodopsin solubilized in dodecyl maltoside (*9*). In that system it was observed that the proton uptake (as measured with a pH-sensitive dye in suspension) is slower than the deprotonation of the Schiff base. In the absorbance signal only one kinetic component was detected. The data were consistent with a pH-dependent k_2. We cannot be sure, of course, that the two sequential isochromic M_{II} species which we called M_{IIa} and M_{IIb} are identical to those described in ref *9*. If they are, the reaction scheme in ROS membranes and dodecyl maltoside micelles is apparently different. This difference is also evident from the fact that in ROS membranes the slower component has the larger activation energy, whereas in the micelle system the opposite was observed (*9*). Assuming that the high activation energy is associated with a structural change, this would occur after proton uptake in ROS membranes, while in micelles the sequence is apparently reversed.

Our simple model for the pH dependence of the kinetics is successful at acid and neutral pH. Small systematic deviations occur, however, in the alkaline pH range. The relative amplitude of the fast electrical component (Figure 4C), for example, does not go completely to zero at alkaline pH as expected from the model (Figure 8C). Moreover, above pH 7.5 the rate of the faster optical component appears to become somewhat faster again (Figures 6, and 8A), contrary to the prediction of the model but in agreement with flash experiments at 23 °C (*6*). Due to the very small amplitude of the absorbance signal in this pH range at 10 °C (Figure 6), these effects could not be properly investigated. In future work the kinetics in the alkaline pH range should therefore be studied at higher temperature where the signal amplitude is larger. The reaction mechanism may be different at alkaline pH, for example, due to a different charge state of the protein or due to the deprotonation of a group indirectly involved in proton uptake.

The fractional value of $n = 0.63$ in $k_0 = k_0'[H^+]^n$ suggests that we are not dealing with a simple protonation reaction in aqueous suspension. The proton uptake takes place at the membrane surface. The surface pH is either larger or smaller than the bulk pH, depending on the sign of the surface charge. The difference between bulk and surface pH depends on the pH and the ionic strength (*33*). The H^+ uptake reaction at the surface depends on the surface pH. The pH we set experimentally is the bulk pH. In the related retinal protein bacteriorhodopsin a proton is taken up at the cytoplasmic surface and this reaction becomes rate-limiting for the decay of the M intermediate at alkaline pH (*18*, *36*). In this case noninteger values of $n = 0.7$ were also observed (*18*, *36*) and could be explained as surface charge effects (*34*). Recent measurements on the ionic strength dependence of the M_I/M_{II} equilibrium in ROS membranes (*29*) suggest that the observed p*K* shift is at least in part due to screening of the positive surface charge on the proton uptake side by the salt.

The pH dependence of the M_I/M_{II} kinetics has been investigated by flash spectroscopy before in the pH range from 6 to 8 between −1 and +15 °C (*8*). In these experiments data could only be collected starting 60 ms after the flash. Under these experimental conditions the relaxation kinetics for the approach to the M_I/M_{II} equilibrium was described by a single exponential. An acceleration of the forward rate constant k_1 by a factor of about 2 was observed when the pH was decreased from 8 to 6 at 15 °C. For the pseudo-first-order forward rate constant $k_1 = k_1'[H^+]^n$ a value of $n = 0.70$ was obtained, which is close to our value of 0.63 obtained with a different kinetic model (eq 1) over the pH range 4−9.

The strong pH dependence reported here for the charge motion associated with the M_{II} formation has not been observed before. At 21 °C only a minor pH dependence in the amplitude associated with the formation of M_{II} was observed over the pH range from 5 to 9 (*15*). No data were reported for the pH dependence of the corresponding rate.

Although all the evidence (activation energies, pH dependence, time range) points to the same molecular origin for the electrical and optical signals, we should point out that under the same experimental conditions the time constants do not agree exactly. Unfortunately it is not possible to perform absorbance and electrical measurements on the same sample to disprove this point. At the same temperature, pH, and ionic strength, the electrical time constants are faster by a factor of 3−5 (pH 7, 10 °C). Whereas the absorption measurements are performed in aqueous suspension, the electrical measurements are carried out with membranes that are adsorbed on a positively charged support. The discrepancy is thus most likely due to environmental effects such as differences in local pH or lateral pressure (*35*). Similar discrepancies were observed for analogous measurements with bacteriorhodopsin (*36*, *18*). In that case the kinetic data from electrical and absorbance measurements were in good agreement when a small pH shift was assumed. Comparing the crossover points of the relative amplitudes of the electrical (Figure 4C) and optical (Figure 8C) measurements a shift of about 0.7 pH unit may be read off.

The kinetics of the rhodopsin photointermediates as monitored by absorbance measurements was recently reviewed (*37*). The kinetics of the rise of M_{II} was studied both at a single wavelength and by optical multichannel methods. Measurements at a single wavelength have the disadvantage that in general more than one intermediate contributes to the signal. This is due to the fact that the spectra of the intermediates overlap strongly. For example, at 380 nm there will be minor contributions from M_I and lumi, as well as from M_{II}. The single-wavelength experiments have the advantage of leading to time-resolved data of higher signal-to-noise ratio, allowing the identification of multiple components. For ROS membranes three time constants were required to fit the high-precision data at 380 nm obtained by signal averaging (*27*). In our single-flash experiments of lower signal-to-noise ratio, only two time constants could be detected. The noise in our data did not allow detection of the smallest (2%) and fastest component, which would be hidden in the noise in the beginning of the trace (Figure 5). To prevent contributions from photochemical reactions of long-living intermediates, we chose to use only single-flash data. Moreover, since we carried out a pH series with a fresh aliquot at each pH, data collection at more than one wavelength turned out to be impractical. In future experiments it will be desirable, however, to perform the pH measurements at a number of wavelengths and to carry out a global fit. A satisfactory and unique reaction scheme for the slow intermediates of rhodopsin has not yet been established (*27*, *28*, *38*, *39*) and further work is clearly required.

Photoreversal from M_{II}. It is well-known that the M_{II} intermediate is photoreversible by blue flashes (*25*). The mechanism of this photo-back-reaction is not known in detail but involves presumably a rapid light-induced isomerization of the chromophore from the all-trans to the 11-cis or 9-cis form, followed by reprotonation of the Schiff base from Glu 113 and the release of protons in the dark. The absorption decrease at 380 nm and increase around 500 nm associated with the photoreversal reflect the reprotonation of the Schiff base. For rhodopsin in dodecyl maltoside micelles the kinetics has two components of approximately equal amplitudes (at 12 °C, pH 6, 130 mM NaCl) (*26*): an unresolved component faster than 1 ms and a component with a "mean time" of around 50 ms. Difference spectra showed that the fast and slow kinetic components are associated with two different final products with λ_{max} values of 470 and 500 nm, respectively (*26*). Similar results were obtained previously with ROS membranes (*25*). In dodecyl maltoside micelles photoreversal is accompanied by proton release, which is, however, approximately 3 times slower ($\tau_{1/2} = 250$ ms, pH 7, 12 °C) than the kinetics of Schiff base reprotonation. Here we observed with ROS membranes that the charge displacement in the photoreversal occurs with only one component with an exponential time constant of 30 ms (pH 7.3, 150 mM KCl, 22 °C). Most likely this is the electrical analogue of the 50 ms component observed in the absorbance measurements. The sign of the charge displacement signal (Figure 3) is consistent with reprotonation of the Schiff base from the same group that first accepted the proton, i.e., Glu 113. The good agreement of our electrical photoreversal kinetics with the previous absorbance work (*26*) supports the idea that electrically one observes the intramolecular reprotonation of the Schiff base, rather than H^+ release. This charge movement is remarkably slow. In bacteriorhodopsin the comparable proton translocation from Asp 85 to the Schiff base in the photoreversal of the M intermediate occurs

in around 200 ns under similar conditions (*40*), i.e., around 5 orders of magnitude faster. It is thus likely that the mechanisms of Schiff base reprotonation differ in these two retinal proteins. In principle, photoreversal could occur from both M_{IIa} and M_{IIb} with different kinetics and final products. This question may be resolved by electrical measurements with double flash (green/blue) excitation, as described for the photoreversal of the M intermediate of bacteriorhodopsin (*40*).

CONCLUSION

The kinetics of the formation of M_{II} in ROS membranes, as monitored by the absorbance change at 380 nm and electrical measurements, is characterized by two apparent time constants. The faster one accelerates by a factor of 8 when the pH is lowered from 7 to 4.0. These results are explained with a model consisting of two sequential equilibria between M_I, M_{IIa}, and M_{IIb}. The pronounced pH dependence of the two apparent time constants and the corresponding amplitudes at eight points between pH 4 and 7.5 was fitted simultaneously to this model with just four microscopic rate constants. A satisfactory description of the kinetic data is only obtained if the forward rate constant between M_I and M_{IIa} is assumed to be proportional to the proton concentration. This result suggests strong coupling between the Schiff base deprotonation and proton uptake at the cytosolic surface of the ROS membrane.

APPENDIX

The kinetic model of eq 1 is described by the following system of coupled differential equations:

$$\frac{\mathrm{d}}{\mathrm{d}t}\begin{pmatrix}M_I\\M_{IIa}\\M_{IIb}\end{pmatrix}=\begin{pmatrix}-k_0 & k_1 & 0\\ k_0 & -k_1-k_2 & k_3\\ 0 & k_2 & -k_3\end{pmatrix}\begin{pmatrix}M_I\\M_{IIa}\\M_{IIb}\end{pmatrix} \quad (2)$$

After flash excitation M_I is formed from lumi with a rate constant that is much larger than the rates k_0, k_1, k_2, k_3. The initial condition is thus to a very good approximation given by

$$\begin{pmatrix}M_I(0)\\M_{IIa}(0)\\M_{IIb}(0)\end{pmatrix}=\begin{pmatrix}1\\0\\0\end{pmatrix} \quad (3)$$

In eq 3 the concentrations are expressed in dimensionless units, as the ratios of the intermediate concentrations to the concentration of excited rhodopsin molecules (*rh**). With this initial condition, the solution of eq 2 is unique and of the form

$$\begin{pmatrix}M_I(t)\\M_{IIa}(t)\\M_{IIb}(t)\end{pmatrix}=\begin{pmatrix}c_{11}\\c_{21}\\c_{31}\end{pmatrix}\mathrm{e}^{-k_u t}+\begin{pmatrix}c_{12}\\c_{22}\\c_{32}\end{pmatrix}e^{-k_d t}+\begin{pmatrix}c_{13}\\c_{23}\\c_{33}\end{pmatrix} \quad (4)$$

k_u, k_d, and 0 are the eigenvalues of the rate matrix on the right-hand side of eq 2 multiplied by −1. The preexponential factors in eq 4 are the corresponding eigenvectors. The c_{ij} depend on the microscopic rate constants of eq 2 and on the initial condition of eq 3. The apparent rates k_u and k_d can be written in compact form using the abbreviation w defined by

$$w=[(k_0+k_1+k_2+k_3)^2-4(k_0k_2+k_0k_3+k_1k_3)]^{1/2} \quad (5)$$

One finds

$$k_u=(k_0+k_1+k_2+k_3+w)/2$$
$$k_d=(k_0+k_1+k_2+k_3-w)/2 \quad (6)$$

The absorbance change at 380 nm is given by

$$\Delta A(t)=\{(\epsilon_{MI}-\epsilon_{rh})M_I(t)+(\epsilon_{MII}-\epsilon_{rh})[M_{IIa}(t)+M_{IIb}(t)]\}\,\mathrm{d}\,rh^* \quad (7)$$

where d is the path length. At 380 nm the contribution of the first term in eq 7 can be neglected since $(\epsilon_{MI}-\epsilon_{rh})$ is only 0.083 of $(\epsilon_{MII}-\epsilon_{rh})$ (*38*). The reason is that both M_I and rhodopsin have a protonated Schiff base. The main contribution comes therefore from the second term:

$$\Delta A(t)=\{(\epsilon_{MII}-\epsilon_{rh})[(c_{21}+c_{31})\mathrm{e}^{-k_u t}+(c_{22}+c_{32})\mathrm{e}^{-k_d t}+c_{23}+c_{33}]\}\,\mathrm{d}\,rh^* \quad (8)$$

Defining $\Delta\epsilon=\epsilon_{MII}-\epsilon_{rh}$, we find for the amplitudes a_u and a_d associated with the faster (k_u) and slower (k_d) rates, respectively,

$$a_u=(c_{21}+c_{31})\Delta\epsilon\,\mathrm{d}\,rh^*=\left[\frac{-k_0k_d(k_0+k_1-k_2-k_3+w)}{2w(k_0k_2+k_0k_3+k_1k_3)}\right]\Delta\epsilon\,\mathrm{d}\,rh^* \quad (9)$$

and

$$a_d=(c_{22}+c_{32})\Delta\epsilon\,\mathrm{d}\,rh^*=\left[\frac{-k_0k_u(k_0+k_1-k_2-k_3-w)}{2w(k_0k_2+k_0k_3+k_1k_3)}\right]\Delta\epsilon\,\mathrm{d}\,rh^* \quad (10)$$

So far the analysis was of general validity. To make further progress it is necessary to make a specific assumption concerning the pH dependence of the microscopic rate constants. When the transition $M_I \rightarrow M_{IIa}$ is coupled to proton uptake, the rate k_0 at approximately constant proton concentration is pseudo-first-order: $k_0=k_0'[H^+]^n=(k_0')\,10^{-n\mathrm{pH}}$. n is the number of protons taken up. At high pH, k_0 goes to zero and we have the following limiting values for w, k_u, k_d, a_u, and a_d:

$$w \xrightarrow{k_0\rightarrow 0} [(k_1+k_2+k_3)^2-4k_1k_3]^{1/2}$$

$$k_u \xrightarrow{k_0\rightarrow 0} (k_1+k_2+k_3+w)/2$$
$$k_d \xrightarrow{k_0\rightarrow 0} (k_1+k_2+k_3-w)/2 \quad (11)$$
$$a_u \xrightarrow{k_0\rightarrow 0} 0, \qquad a_d \xrightarrow{k_0\rightarrow 0} 0$$

At high pH the apparent rates thus become pH-independent, whereas the corresponding amplitudes go to zero (see Figure 8). At low pH, $k_0 \rightarrow \infty$ and we have the following limiting values for w, k_u, k_d, a_u, and a_d:

$$w \xrightarrow{k_0 \to \infty} [k_0^2 + 2k_0(k_1 - k_2 - k_3) + ...]^{1/2} \approx k_0 + k_1 - k_2 - k_3$$

$$k_u \xrightarrow{k_0 \to \infty} k_0 + k_1, \qquad k_d \xrightarrow{k_0 \to \infty} k_2 + k_3 \tag{12}$$

$$a_u \xrightarrow{k_0 \to \infty} -\Delta\epsilon \, d \, rh^*, \qquad a_d \xrightarrow{k_0 \to \infty} 0$$

Thus at low pH the two equilibria uncouple with k_u and k_d given by the relaxation rate for the first and second equilibrium, respectively. The slower rate k_d is pH-independent and the corresponding amplitude a_d approaches zero. The faster rate k_u approaches $k_0 = k_0'[H^+]^n$ and becomes faster with decreasing pH. The corresponding amplitude a_u dominates (see Figure 8).

The equilibrium concentration of M_I, which can be easily measured, is of particular interest. It is given according to eq 4 by $M_I(\infty)$:

$$M_I(\infty) = c_{13} = \frac{k_1 k_3}{k_1 k_3 + k_0 k_2 + k_0 k_3} \tag{13}$$

With $k_0 = k_0'[H^+]^n$ we can write this in the following way:

$$M_I(\infty) = \frac{1}{1 + 10^{\{(1/n)\log[[(k_2 + k_3)/k_1 k_3]k_0'] - pH\}n}} \tag{14}$$

Equation 14 has the form of a Henderson−Hasselbalch equation with apparent pK given by

$$pK = \frac{1}{n} \log\left(\frac{k_2 + k_3}{k_1 k_3} k_0'\right) \tag{15}$$

The apparent pK is determined by the intrinsic rate constants, which we obtained by fitting the pH-dependent apparent rates and amplitudes. Using the fit values at 10 °C, 150 mM KCl ($k_0' = 147\,000$ s^{-1}, $k_1 = 63$ s^{-1}, $k_2 = 48$ s^{-1}, $k_3 = 4$ s^{-1}, $n = 0.63$), we obtain a pK of 7.14. This is in excellent agreement with the value of 7.3 recently obtained for ROS membranes under the same conditions (*29*).

REFERENCES

1. Khorana, H. G. (1992) *J. Biol. Chem. 267*, 1−4.
2. Hargrave, P. A., and McDowell, J. H. (1992) *FASEB J. 6*, 2323−2331.
3. Ottolenghi, M., and Sheves, M. (1995) *Isr. J. Chem. 35*, 193−515.
4. Jäger, F., Fahmy, K., Sakmar, T. P., and Siebert, F. (1994) *Biochemistry 33*, 10878−10882.
5. Matthews, R. G., Hubbard, R., Brown, P. K., and Wald, G. (1963) *J. Gen. Physiol. 38*, 215−240.
6. Emrich, H. M., and Reich, R. (1974) *Z. Naturforsch. 29C*, 577−591.
7. Bennett, N. (1980) *Eur. J. Biochem. 111*, 99−103.
8. Parkes, J. H., and Liebman, P. A. (1984) *Biochemistry 23*, 5054−5061.
9. Arnis, S., and Hofmann, K. P. (1993) *Proc. Natl. Acad. Sci. U.S.A. 90*, 7849−7853.
10. Moltke, S., Alexiev, U., and Heyn, M. P. (1995) *Isr. J. Chem. 35*, 401−414.
11. Lindau, M., Hochstrate, P., and Rüppel, H. (1980) *FEBS Lett. 112*, 17−20.
12. Drachev, L. A., Kalmakarov, G. R., Kaulen, A. D., Ostrovsky, M. A., and Skulachev, V. P. (1981) *Eur. J. Biochem. 117*, 471−481.
13. Lindau, M., and Rüppel, H., (1983) *Photobiochem. Photobiophys. 5*, 219−228.
14. Bauer, P. J., Bamberg, E., and Fahr, A. (1984) *Biophys. J. 46*, 111−116.
15. Lindau, M., and Rüppel, H. (1985) *Photobiochem. Photobiophys. 9*, 43−56.
16. McDowell, J. H., and Kühn, H. (1977) *Biochemistry 16*, 4054−4060.
17. Yamanaka, G., Eckstein, F., and Stryer, L. (1985) *Biochemistry 24*, 8094−8101.
18. Otto, H., Marti, T., Holz, M., Mogi, T., Lindau, M., Khorana, H. G., and Heyn, M. P. (1989) *Proc. Natl. Acad. Sci. U.S.A. 86*, 9228−9232.
19. Holz, M., Lindau, M., and Heyn, M. P. (1988) *Biophys. J. 53*, 623−633.
20. Moltke, S., and Heyn, M. P. (1995) *Biophys. J. 69*, 2066−2073.
21. Dickopf, S., Alexiev, U., Krebs, M. P., Otto, H., Mollaaghababa, R., Khorana, H. G., and Heyn, M. P. (1995) *Proc. Natl. Acad. Sci. U.S.A. 92*, 11519−11523.
22. Shieh, T., Han, M., Sakmar, T. P., and Smith, S. O. (1997) *J. Mol. Biol. 269*, 373−384.
23. Pogozheva, I. D., Lomize, A. L., and Mosberg, H. I. (1997) *Biophys. J. 70*, 1963−1985.
24. Herzyk, P., and Hubbard, R. E. (1998) *J. Mol. Biol. 281*, 741−754.
25. Williams, T. (1968) *Vision Res. 8*, 1457−1466.
26. Arnis, S., and Hofmann, K. P. (1995) *Biochemistry 34*, 9333−9340.
27. Straume, M., Mitchell, D. C., Miller, J. L., and Litman, B. J. (1990) *Biochemistry 29*, 9135−9142.
28. Thorgeirsson, T. E., Lewis, J. W., Wallace-Williams, S. E., and Kliger, D. S. (1993) *Biochemistry 32*, 13861−13872.
29. Delange, F., Merkx, M., Bovee-Geurts, P. H. M., Pistorius, A. M. A., and De Grip, W. J. (1997) *Eur. J. Biochem. 243*, 174−180.
30. Sakmar, T. P., Franke, R. R., and Khorana, H. G. (1989) *Proc. Natl. Acad. Sci. U.S.A. 86*, 8309−8313.
31. Arnis, S., Fahmy, K., Hofmann, K. P., and Sakmar, T. P. (1994) *J. Biol. Chem. 269*, 23879−23881.
32. Brown, L. S., Kamikubo, H., Zimányi, L., Kataoka, M., Tokunaga, F., Verdegem, P., Lugtenburg, J., and Lanyi, J. K. (1997) *Proc. Natl. Acad. Sci. U.S.A. 94*, 5040−5044.
33. Szundi, I., and Stoeckenius, W. (1989) *Biophys. J. 56*, 369−383.
34. Miller, A., and Oesterhelt, D. (1990) *Biochim. Biophys. Acta 1020*, 57−66.
35. Brown, M. F. (1994) *Chem. Phys. Lipids 73*, 159−180.
36. Holz, M., Drachev, L. A., Mogi, T., Otto, H., Kaulen, A. D., Heyn, M. P., Skulachev, V. P., and Khorana, H. G. (1989) *Proc. Natl. Acad. Sci. U.S.A. 86*, 2167−2171.
37. Kliger, D. S., and Lewis, J. W. (1995) *Isr. J. Chem. 35*, 289−307.
38. Szundi, I., Lewis, J. W., and Kliger, D. S. (1997) *Biophys. J. 73*, 688−702.
39. Tachibanaki, S., Imai, H., Mizukami, T., Okada, T., Imamoto, Y., Matsuda, T., Fukada, Y., Terakita, A., and Shichida, Y. (1997) *Biochemistry 36*, 14173−14180.
40. Dickopf, S., and Heyn, M. P. (1997) *Biophys. J. 73*, 3171−3181.
41. Thorgeirsson, T. E., Lewis, J. W., Wallace-Williams, S. E., and Kliger, D. S. (1992) *Photochem. Photobiol. 56*, 1135−1144.

BI981879M